

MIT Open Access Articles

*Reduced-order precursors of rare events
in unidirectional nonlinear water waves*

The MIT Faculty has made this article openly available. **Please share** how this access benefits you. Your story matters.

Citation: Cousins, Will, and Themistoklis P. Sapsis. "Reduced-Order Precursors of Rare Events in Unidirectional Nonlinear Water Waves." *Journal of Fluid Mechanics* 790 (February 11, 2016): 368–388.

As Published: <http://dx.doi.org/10.1017/jfm.2016.13>

Publisher: Cambridge University Press

Persistent URL: <http://hdl.handle.net/1721.1/101436>

Version: Author's final manuscript: final author's manuscript post peer review, without publisher's formatting or copy editing

Terms of use: Creative Commons Attribution-Noncommercial-Share Alike



Reduced order precursors of rare events in unidirectional nonlinear water waves

Will Cousins and Themistoklis P. Sapsis[†]

Department of Mechanical Engineering, Massachusetts Institute of Technology, 77
Massachusetts Ave., Cambridge, MA, USA

(Received xx; revised xx; accepted xx)

We consider the problem of short-term prediction of rare, extreme water waves in irregular unidirectional fields, a critical topic for ocean structures and naval operations. One possible mechanism for the occurrence of such rare, unusually-intense waves is nonlinear wave focusing. Recent results have demonstrated that random localizations of energy, induced by the linear dispersive mixing of different harmonics, can grow significantly due to modulation instability. Here we show how the interplay between i) modulation instability properties of localized wave groups and ii) statistical properties of wave groups that follow a given spectrum defines a critical length scale associated with the formation of extreme events. The energy that is locally concentrated over this length scale acts as the ‘trigger’ of nonlinear focusing for wave groups and the formation of subsequent rare events. We use this property to develop inexpensive, short-term predictors of large water waves, circumventing the need for solving the governing equations. Specifically, we show that by merely tracking the energy of the wave field over the critical length scale allows for the robust, inexpensive prediction of the location of intense waves with a prediction window of 25 wave periods. We demonstrate our results in numerical experiments of unidirectional water wave fields described by the Modified Nonlinear Schrodinger equation. The presented approach introduces a new paradigm for understanding and predicting intermittent and localized events in dynamical systems characterized by uncertainty and potentially strong nonlinear mechanisms.

1. Introduction

Understanding and predicting large magnitude, nonlinear water waves is one of the most challenging topics for ocean engineering both because of the catastrophic impact they can have on ocean engineering structures (e.g. ships and offshore platforms) and naval operations, but also because of the lack of specialized mathematical tools for the analysis of the underlying physics (Dysthe *et al.* 2008; Akhmediev & Pelinovsky 2010; Müller *et al.* 2005; Xiao *et al.* 2013). This is because nonlinear water wave dynamics are characterized both by the existence of inherent uncertainty (expressed in the form of phase uncertainty between different Fourier modes) and also in the form of strong nonlinearities and associated energy transfers between modes. The latter can be activated locally and intermittently, leading to unusually high magnitude waves that emerge out of the complex background wave field.

An extreme form of such dynamical evolution is the case of freak or rogue waves with wave height which can be as large as eight times the standard deviation of the surrounding wave field (Onorato *et al.* 2005; Dysthe *et al.* 2008). Waves of this magnitude have caused considerable damage to ships, oil rigs, and human life (Haver 2004; Liu 2007). In addition,

[†] Email address for correspondence: sapsis@mit.edu

many naval operations e.g. transfer of cargo between ships moored together in a sea base, landing on aircraft carriers, or path planning of high-speed surface vehicles require short-term prediction of the surrounding wave field. To make such predictions, unusually high wave elevations must be forecasted reliably.

One mechanism for the occurrence of such rare, unusually-intense wave elevations is nonlinear wave focusing (Janssen 2003; Onorato *et al.* 2002a; Cousins & Sapsis 2015). For deep water waves a manifestation of this focusing is the well-known Benjamin-Feir instability of a plane wave to small sideband perturbations. This instability, which has also been demonstrated experimentally (Chabchoub *et al.* 2011), generates huge coherent structures by soaking up energy from the nearby field (Benjamin & Feir 1967; Zakharov 1968; Osborne *et al.* 2000). Cousins & Sapsis (2015) demonstrated that even imperfect background conditions, i.e. completely different from the idealized plane wave setup of the Benjamin-Feir instability, can still lead to important wave focusing and rare events. In particular, it was analytically shown and numerically demonstrated for unidirectional wavetrains that there is a critical combination of wave group length scales and amplitudes which will lead to wave focusing and thus unusually high elevations. In contrast to the standard BF mechanism these instabilities are initiated because of sufficiently large spatially localized energy.

Such energy localization, which can ‘trigger’ nonlinear wave focusing can occur as the result of random relative phases between different harmonics. This phase randomness is mainly introduced by the mixing of different harmonics due to their linear dispersive propagation. Thus, the linear propagation of water waves can locally create conditions that will lead to nonlinear focusing and subsequent rare events. It is clear that this perspective provides a scenario in which the unstable extreme wave events are isolated occurrences of strongly nonlinear focusing events initiated by the linear or weakly nonlinear background.

Therefore, *on the one hand we have the nonlinear wave mechanics that define which localized wave groups will focus because of modulation instabilities, while on the other hand we have the power spectrum that defines what wave groups can form because due to random phase difference between harmonics.* The scope of this work is to combine these two perspectives in order to derive precursors of rare events that will take into account both the nonlinear mechanics of water waves (in particular the modulation instability) but also the spectral or statistical properties of the wave field. In particular, we show how the interplay between i) modulation instability properties of localized wave groups and ii) statistical properties of wave groups associated with a given spectrum defines a critical length scale that is related with the occurrence of strongly nonlinear interactions and the formation of extreme events. The energy that is locally concentrated over this length scale acts essentially as the ‘trigger’ of nonlinear focusing of wave groups.

We use this property to derive short-term precursors for the occurrence of large water waves, circumventing the need for solving the governing equations. To quantify the probability of occurrence of specific wave group from a given spectrum we use a scale-selection algorithm (Lindeberg 1998). This statistical analysis is combined with an analytical nonlinear stability criterion for focusing of localized wavegroups (Cousins & Sapsis 2015) to yield a reliable, computationally inexpensive forecast of the subsequent growth for each wave group in the field. In a second stage, we demonstrate that merely tracking the energy of the wave field over the critical length scale defined by the interplay between statistics and nonlinearity allows for an even cheaper and robust forecast of upcoming intense nonlinear wave elevations, with a prediction window on the order of 25 wave periods. We demonstrate our results in numerical experiments involving unidirectional water wave fields described by the Modified Nonlinear Schrodinger equation.

Our proposed predictive method reveals and directly uses the low-dimensional character of the domain of attraction of these rare water waves. In particular, despite the distribution of the background energy over a wide range of scales, the ‘trigger’ of nonlinear focusing is essentially low-dimensional and to this end it can be used as an inexpensive way to estimate the probability for a rare event in the near future. Our scheme is robust, performing well even with noise and irregularity in the wave field. Furthermore, the presented approach introduces a new paradigm for handling spatiotemporal rare events in dynamical systems with inherent uncertainty by providing an efficient description of the ‘trigger’ that leads to those rare events through the careful study of the synergistic action between uncertainty and nonlinearity.

We stress that our method differs significantly from previously described predictive schemes. For example, the inverse scattering approach of Islas & Schober (2005) is, in its proposed form, limited to NLS. Our wave group based scheme easily applies to the more accurate modified NLS equation where such analytical tools are not available. Also, our scheme is similar in spirit to the quasi-determinism (QD) theory of Boccotti (2008), which extends the observation that profiles of large amplitude waves resemble the autocorrelation function (Lindgren 1970; Boccotti 1983). Boccotti’s QD theory is linear and has been extended to include second order effects by Fedele & Tayfun (2009). Although second order quasi-determinism agrees well with many oceanic observations, our scheme allows us to perform prediction of rare events occurring due to nonlinear focusing effects induced by wave-wave interactions which are associated with highly nonlinear regimes where current analytical methods are limited.

2. Extreme Events in Envelope Equations

In this work, we consider irregular waves traveling on the surface of a fluid of infinite depth. A typical approach for modeling this phenomena is to assume incompressible, irrotational, inviscid flow, which gives Laplace’s equation for the velocity potential. This equation is paired with two boundary conditions on the surface: a pressure condition and a kinematic one (a particle initially on the free surface remains so). This model agrees well with laboratory experiments (Wu *et al.* 1998), and faithfully reproduces the classical $k^{-5/2}$ spectral tail observed in deep water (Onorato *et al.* 2002*b*). Although some care is required to numerically deal with the free surface, this fully nonlinear model may be solved numerically with reasonable computational effort, particularly in one space dimension (Dommermuth & Yue 1987; Craig & Sulem 1993; Dyachenko *et al.* 1996; Choi & Camassa 1999). However, the presence of the free surface makes analysis of the underlying dynamics challenging.

Here we consider approximate equations governing the evolution of the wave envelope, the Nonlinear Schrodinger Equation (NLS) (Zakharov 1968) and the Modified Nonlinear Schrodinger Equation (MNLS) of (Dysthe 1979). Both NLS and MNLS can be derived via a perturbation approach from the fully nonlinear model under assumptions of small steepness and slow variation of the wave envelope. Although forms of these equations exist in a full two-dimensional setting, here we consider wave fields varying only in the direction of propagation. The NLS equation, in nondimensionalized coordinates, reads

$$\frac{\partial u}{\partial t} + \frac{1}{2} \frac{\partial u}{\partial x} + \frac{i}{8} \frac{\partial^2 u}{\partial x^2} + \frac{i}{2} |u|^2 u = 0 \quad (2.1)$$

where $u(x, t)$ is the wave envelope. To leading order the surface elevation is given by $\eta(x, t) = \Re[u(x, t)e^{i(x-t)}]$. Equation (2.1) has been nondimensionalized with $x = k_0 \tilde{x}$, $t =$

$\omega_0 \tilde{t}, u = k_0 \tilde{u}$, where \tilde{x}, \tilde{t} , and \tilde{u} are physical space, time and envelope. k_0 is the dominant spatial frequency of the surface elevation, and $\omega_0 = \sqrt{gk_0}$.

Our primary interest in this work is the Modified NLS equation, which is a higher order approximation of the fully nonlinear model,

$$\frac{\partial u}{\partial t} + \frac{1}{2} \frac{\partial u}{\partial x} + \frac{i}{8} \frac{\partial^2 u}{\partial x^2} - \frac{1}{16} \frac{\partial^3 u}{\partial x^3} + \frac{i}{2} |u|^2 u + \frac{3}{2} |u|^2 \frac{\partial u}{\partial x} + \frac{1}{4} u^2 \frac{\partial u^*}{\partial x} + iu \frac{\partial \phi}{\partial x} \Big|_{z=0} = 0 \quad (2.2)$$

where ϕ is the velocity potential and $\partial \phi / \partial x \Big|_{z=0} = -\mathcal{F}^{-1} [|k| \mathcal{F}[|u|^2]] / 2$. \mathcal{F} denotes the Fourier transform. The MNLS equation has been shown to reproduce laboratory experiments reasonably well (Lo & Mei 1985; Goullet & Choi 2011). There are even higher order envelope equations, such as the Broadband Modified NLS Equation (BMNLS) (Trulsen & Dysthe 1996) as well as the more recent compact Zakharov equation (Dyachenko & Zakharov (2011)). The latter is valid for third order nonlinearities and it does not have restrictions on the spectral bandwidth (Fedele (2014)). However, we do not discuss these equations here. Although there are considerable differences between NLS and MNLS, we found minimal differences between simulations of MNLS and BMNLS. Dysthe *et al.* (2003) also found similar agreement between MNLS and BMNLS.

These envelope equations, as well as the fully nonlinear water wave model, admit periodic plane wave solutions. Interestingly, these plane wave solutions are unstable to side-band perturbations ((Benjamin & Feir 1967), see also (Zakharov 1968)), a phenomenon termed the Benjamin-Feir instability. This instability has a striking manifestation. Energy is ‘‘sucked up’’ from the nearby field to produce a large amplitude coherent structure, containing a wave 2.4-3 times larger than the surrounding background field (Osborne *et al.* 2000). This behavior has been shown numerically in envelope equations (Yuen & Ferguson 1978; Dysthe & Trulsen 1999) as well as in the fully nonlinear formulation (Henderson *et al.* 1999). Furthermore, a number of experiments confirm these numerical predictions (Chabchoub *et al.* 2011, 2012).

However, in realistic physical settings, the water surface is not merely a plane wave—energy is distributed over a range of frequencies. To this end, we consider extreme waves emerging out of a background with Gaussian spectra and random phases, that is

$$u(x, 0) = \sum_{-N/2+1}^{N/2} \sqrt{2\Delta_k F(k\Delta_k)} e^{i(\omega_k x + \xi_k)}, \quad F(k) = \frac{\epsilon^2}{\sigma\sqrt{2\pi}} e^{-\frac{k^2}{2\sigma^2}} \quad (2.3)$$

where ξ_k are independent, uniformly distributed random phases. Here we adopt the definition of an extreme wave as any instance where $|u| > H_E = 4\epsilon$ (as defined above ϵ is the standard deviation of the surface elevation). In these irregular wave fields, it is well known that the critical quantity for extreme event formation is the Benjamin-Feir Index, which is the ratio of the energy level of the field to its bandwidth (Janssen 2003). If the Benjamin-Feir Index is large enough, then nonlinear interactions dominate, leading to the appearance of large amplitude coherent structures and heavy-tailed statistics for the elevation (Alber 1978; Crawford *et al.* 1980; Dysthe *et al.* 2003; Janssen 2003; Onorato *et al.* 2005).

We solve the MNLS equation numerically using a Fourier method in space. The use of periodic boundary conditions is of course artificial, but is a standard convention. We take our spatial domain to be 128 wavelengths (256π), large enough to avoid any box-size effects. We use a 4th order Runge-Kutta exponential time differencing scheme (Cox & Matthews 2002; Grooms & Majda 2014). This scheme requires evaluation of the function $\phi(z) = (e^z - 1)/z$. Naive computation of ϕ can suffer from numerical cancellation error

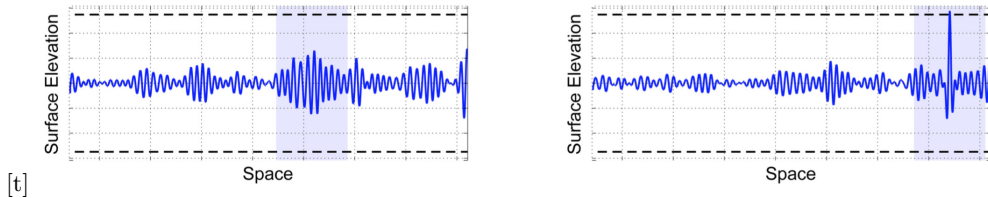


FIGURE 1. Large amplitude coherent structures (right), which emerges via focusing of a localized wave group (left).

for small z (Kassam & Trefethen 2005). We use a Pade approximation code from the EXPINT software package, which does not suffer from such errors (Berland *et al.* 2007). We use 2^{10} Fourier modes with a time step of 0.025; results in this work were insensitive to further refinement in grid size.

3. Localized Wave Group Evolution

A large Benjamin-Feir Index indicates that the extreme events are more likely than Gaussian statistics would suggest. However, the Benjamin-Feir Index does *not* provide any specific information on precisely where an extreme event will occur. Thus, in order to develop a scheme providing precise spatiotemporal predictions we must develop a more precise indicator than the BFI. In high BFI seas, extreme events are triggered by the nonlinear focusing of localized wave groups (Fedele 2008). Figure 1 displays such an example of extreme event formation by focusing of localized groups. In this case we see that a localized group focuses, narrowing in width and doubling in amplitude, yielding an extreme event.

To better understand this mechanism, in (Cousins & Sapsis 2015) we studied the evolution of isolated wave groups. We review these results describing the evolution of hyperbolic secant initial data:

$$u(x, 0) = A \operatorname{sech}(x/L).$$

For the NLS equation on zero background this family of envelopes give rise to the Satsuma-Yajima breathers that have been observed experimentally in the context of NLS and MNLS (Chabchoub *et al.* (2013)). Due to the invariance of the envelope equations we take A real with no loss of generality. We investigate the evolution of such groups as a function of amplitude A and length scale L . In particular, we are interested in whether or not a group will focus and, if it does, the degree by which the group amplitude is magnified.

We emphasize the difference between the instability occurring due to initially localized energy (and zero background) and the classical modulation instability of plain waves. Specifically, in the classical Benjamin-Feir instability the aim is to understand when and how energy is transferred from the background wave train to a localized wave group that has the form of a breather solution. In this case the conditions of occurrence and lengthscale of the instability depend on the amplitude of the plane wave. However, for our study assuming a perfect plane wave as background reservoir of energy is not realistic. It is rather more rational to understand if and how energy is transferred from an already localized wave group to smaller scales, resulting in rare events. These localized wave groups are the result of random phases between harmonics caused by linear dispersion. To this end we will focus our attention on the modulation instability properties of individual and isolated wave groups. Similar questions were asked by Adcock *et al.* in the context of

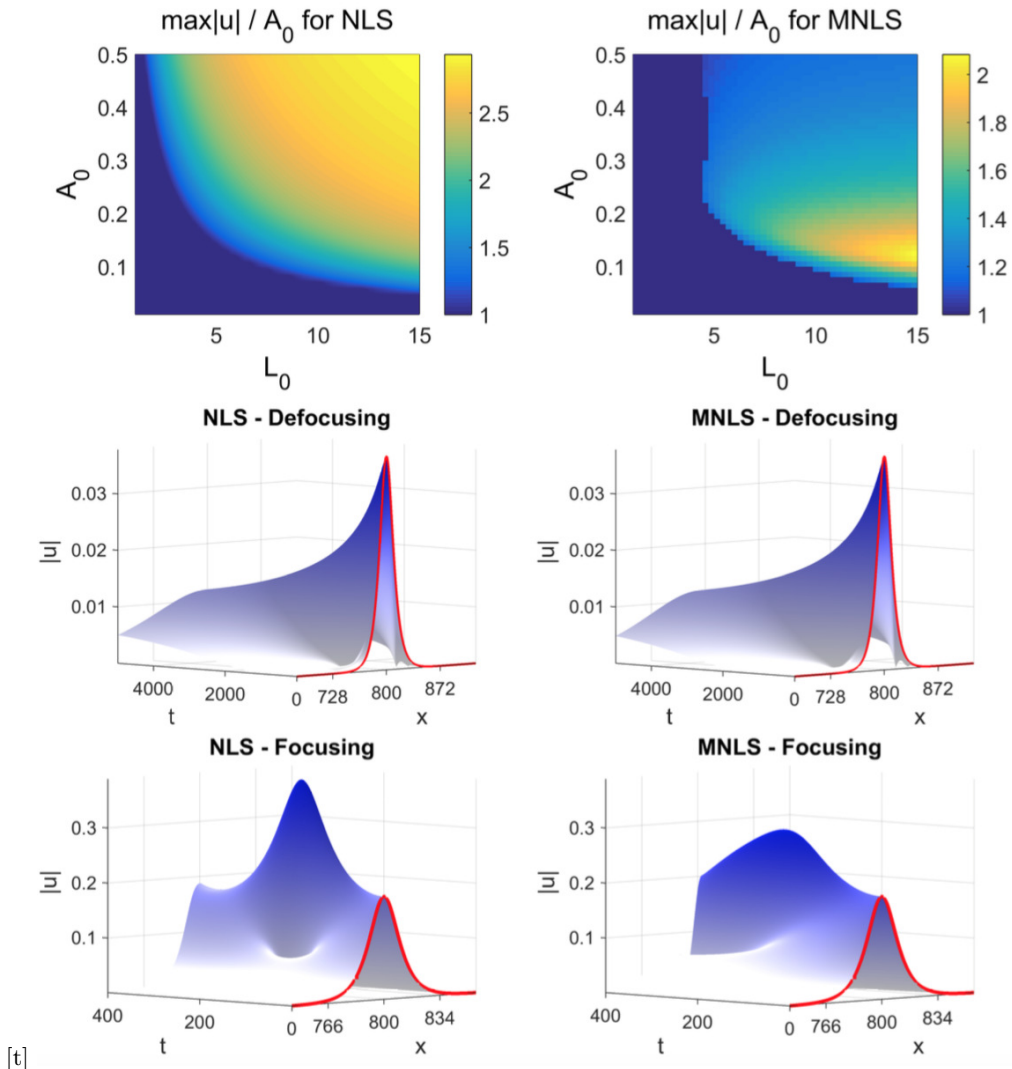


FIGURE 2. Top: Amplitude growth factors for localized groups in NLS (left) and MNLS (right). Middle: examples of defocusing, amplitude decreasing groups for NLS (left) and MNLS (right). Bottom: examples of focusing, amplitude increasing groups for NLS and MNLS. The initial conditions for the simulations displayed in the bottom left and bottom right are identical. Although both groups focus, the amplitude grows considerably less in MNLS than in NLS.

the one-dimensional NLS (Adcock & Taylor 2009) as well as NLS and the fully nonlinear model in two dimensions (Adcock *et al.* 2012).

To answer these questions, we numerically evolve hyperbolic secant initial data for many values of A and L for NLS and MNLS. To measure the degree of focusing a group undergoes, we compute the value of the first spatiotemporal local maximum of $|u|$, and termed this value $u_{max}(A, L)$. For a defocusing group however (middle row, Figure 2), this local maximum will occur at $x = 0, t = 0$ and we trivially have $u_{max}(A, L) = A$. For a focusing group (bottom row, Figure 2), the group will contract and increase in amplitude. The group amplitude will eventually reach a maximum and then demodulate, decreasing in amplitude. To make the focusing behavior clear, in the top two panes of Figure 2 we

plot the amplitude growth factor $\frac{1}{A}u_{\max}(A, L)$ for NLS (top left pane) and MNLS (top right pane). This amplitude growth factor describes the degree of focusing which has occurred, with a value of 1 indicating that the group does not grow in amplitude.

We observe that for both NLS and MNLS, there are a range of groups that focus considerably. However, there are stark differences between group evolution in the two equations owing to the lack of scale invariance in the MNLS equation. In MNLS, the set of focusing groups is smaller compared with NLS, and many groups that do focus do so to a smaller degree (see example in bottom row, Figure 2). Particularly, in MNLS there is a smallest focusing length scale where groups thinner than this scale do not focus, regardless of how large their initial amplitude may be. The scale invariance of NLS, however, precludes such behavior. A similar lack of focusing behavior at small group length scales was observed by Henderson *et al.* in numerical simulations of the fully nonlinear model in one space dimension (Henderson *et al.* 1999).

The presented modulation instability analysis of localized wave groups will be the first ingredient for the derivation of precursors of rare wave events. It provides information about the wave groups that can lead to rare events because of nonlinear focusing effect but it does not provide information about the likelihood of such wave groups. This information will be extracted using a statistical analysis from the spectrum of the wave field.

4. Probability of Critical Wave Groups in Irregular Wave Fields

In a particular sea state dispersion effects create random mixing of different harmonics. To this end, all groups do not occur with equal likelihood—the probability of a particular group occurring is determined by the spectral properties of the field. For example, in a Gaussian spectrum the spatial field will contain groups unlikely to focus if the energy level ϵ is small (low amplitude groups) or if the spectral bandwidth σ is large (small length scale groups). Thus, the frequency and nature of the unstable wave groups in a particular field results from the interplay of the nonlinear dynamical properties of the system (expressed as modulation instabilities of wave groups) and the statistical properties of the background field (expressed by the spectrum).

We now describe a computational procedure to quantify for any given spectrum the probability of occurrence of a wave group of a given amplitude and length scale. To compute this probability density function we use an ensemble approach. Using the random phase model (2.3) we generate realizations that follow the given spectrum. For each realization we use a scale selection algorithm to identify coherent wave groups as well as their associated length scales and amplitudes (see Appendix A for details on the scale selection algorithm). In the top pane of Figure 3, we display an example of such a random realization field $|u(x)|$ as well as the groups identified by the group detection algorithm, showing that this algorithm appropriately picks out the dominant groups. We then compute the joint probability density of group amplitude and length scale by applying this group identification algorithm to 50,000 realizations of Gaussian spectrum random fields.

The described step has very low computational cost since it does not involve the numerical solution of dynamical equations but only the statistical analysis of wave realizations that follow a given spectrum. It is the second ingredient, the statistical component of our analysis, which we will now combine with the modulation instability analysis of localized wavegroups presented in the previous section. More specifically, using the analysis for the evolution of localized wave groups we determine, for each length scale L , the smallest group amplitude required to ‘trigger’ an extreme event. That is, if the

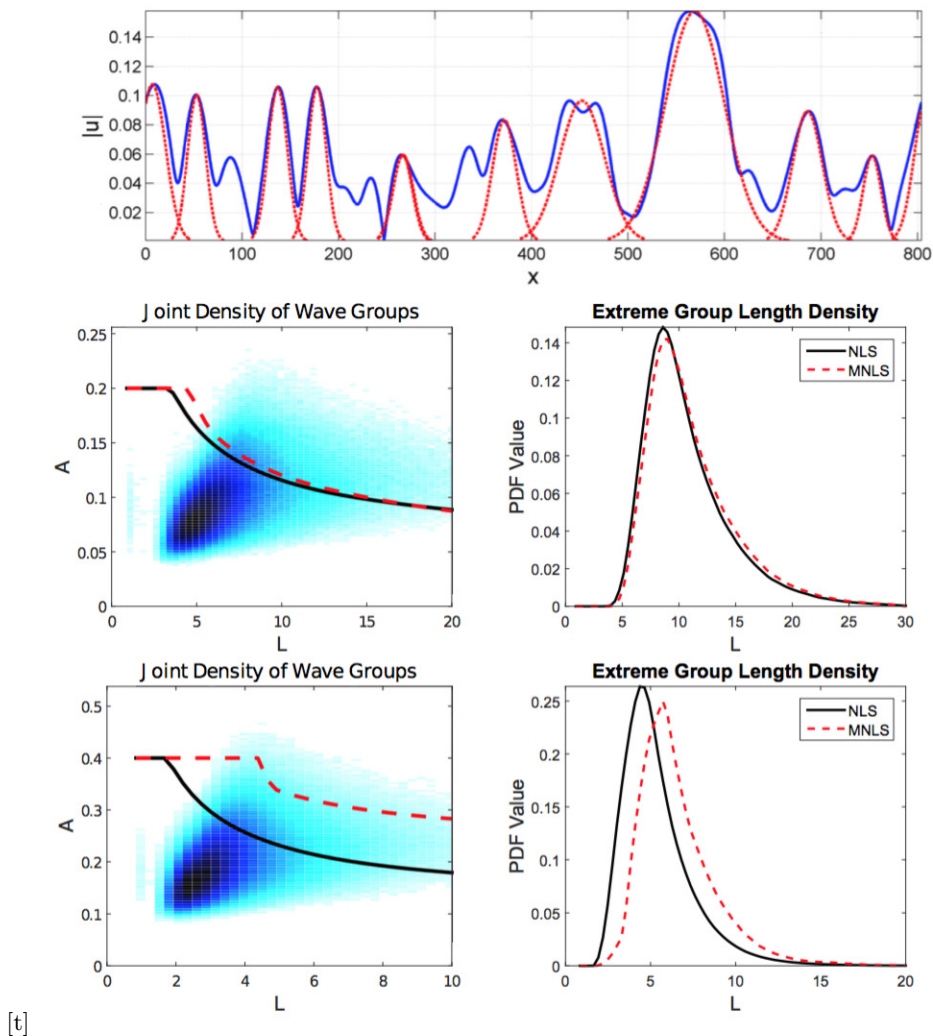


FIGURE 3. Top: Dominant wave groups (red, dashed) determined by applying the group detection algorithm to the field $|u(x)|$ (blue, solid). Middle Row: Joint density of wave group amplitude and length scale (left); Length scale density for extreme ‘triggering’ groups (right), $\text{BFI} = 1.4$, $\epsilon = 0.05$, $\sigma = 0.1$. Bottom row: idem for $\text{BFI} = 1.4$, $\epsilon = 0.1$, $\sigma = 0.2$. In each joint density plot we overlay the curve that separates groups that would focus (if isolated) to form extreme events, NLS curve is black, solid, MNLS curve is red, dashed.

extreme event threshold is $H_E = 4\epsilon$, we find, for each L , the smallest A such that $u_{\max}(A, L) \geq H_E$. Denoting this amplitude as A^* , we trivially have $A^* \leq H_E$. This procedure describes a curve $A^*(L)$, where isolated groups located above this curve in the (L, A) plane would yield an extreme event, and those below this curve would not. Note that wave groups with sufficiently small initial length scales L will never undergo through nonlinear focusing. For these length scales the only wave groups that can reach amplitudes as large as H_E are the ones that start with $A^*(L) = H_E$. This observation explains the plateau that occurs for small L .

In Figure 3 we overlay this curve (that expresses dynamical properties of nonlinear wave groups) over the joint density of group amplitude and length scale (that expresses

statistical properties of the waves spectrum). For a given spectrum, we may determine the frequency and nature of extreme event-triggering groups (i.e. those lying above the respective curves in Figure 3). As expected, increasing the energy level or decreasing the spectral bandwidth increases the number of these extreme-triggering groups. This analysis provides a concrete, wave-group based explanation of the development of heavy tails via nonlinear interactions in high BFI regimes. However, unlike traditional BFI-based analysis, this wave group analysis directly incorporates the lack of scale invariance in MNLS. This is clear from Figure 3 (middle, bottom rows) where we display (A, L) densities for two different spectra with the same BFI. We note the scale invariance property of NLS (note that the two black curves are identical, albeit the axes rescale) and how this contrasts to the corresponding curves (red dashed lines) for the MNLS, which change between the two spectra even though the BFI index remains the same.

The main benefit of this statistical instability analysis allows us to characterize the properties of extreme event-triggering groups in a maximum likelihood sense. Specifically, for a given spectrum, we can compute the density of the length scale of groups that would generate extreme events (i.e. those lying above the curves in the left column of Figure 3). In Figure 3 (right column) we display examples of these length scale densities for the two different spectra. The concentration of these densities around their peak value suggests that for a given spectrum there is a most likely extreme event-triggering length scale, L_E . As the distribution is fairly narrow, we expect that the majority of extreme events that occur will be triggered by localization at length scales close to L_E . In Section 5, we will use this fact to develop a predictive scheme based on projecting the field onto an appropriately tuned set of Gabor wavelets.

5. Precursors of Extreme Events

In this section, we describe the central result of this paper that is the derivation of precursors for extreme events in nonlinear water waves. These precursors allows for the detection of instabilities at their very early stages and therefore lead to the prediction of rare events without the need to solve the full envelope equations.

We describe two precursor forms. First, we develop an algorithm to predict extreme events by identifying the dominant wave groups in a given field, and use our results from Section 3 regarding localized groups that can ‘trigger’ an extreme event. Second, we develop a scheme based on projecting the field onto a carefully tuned set of Gabor modes. We find that large values of a certain Gabor coefficient indicate that an upcoming extreme event is likely. This Gabor-based scheme is nearly as reliable as the group detection scheme, yet requires a remarkably smaller computational cost.

5.1. Prediction by Wave Group Identification

Here we describe a straightforward scheme for advance prediction of extreme events via wave group identification. For a given wave field, we apply the group identification algorithm described in Appendix A to the envelope. This gives the spatial location, amplitude A , and length scale L of each wave group. We then predict the future focused amplitude of the group by evaluating $u_{max}(A, L)$, where u_{max} is the numerically constructed function from our prior study of localized groups in Section 3. If $u_{max}(A, L)$ is at least 95% of the extreme event threshold H_E , then we predict that an extreme event will occur. We choose this conservative prediction threshold in order to minimize the number of false negatives (extreme events that we fail to predict).

In Figure 4, we display an example output of our predictive scheme for a simulation of MNLS with initial conditions generated via a Gaussian spectrum with random phases

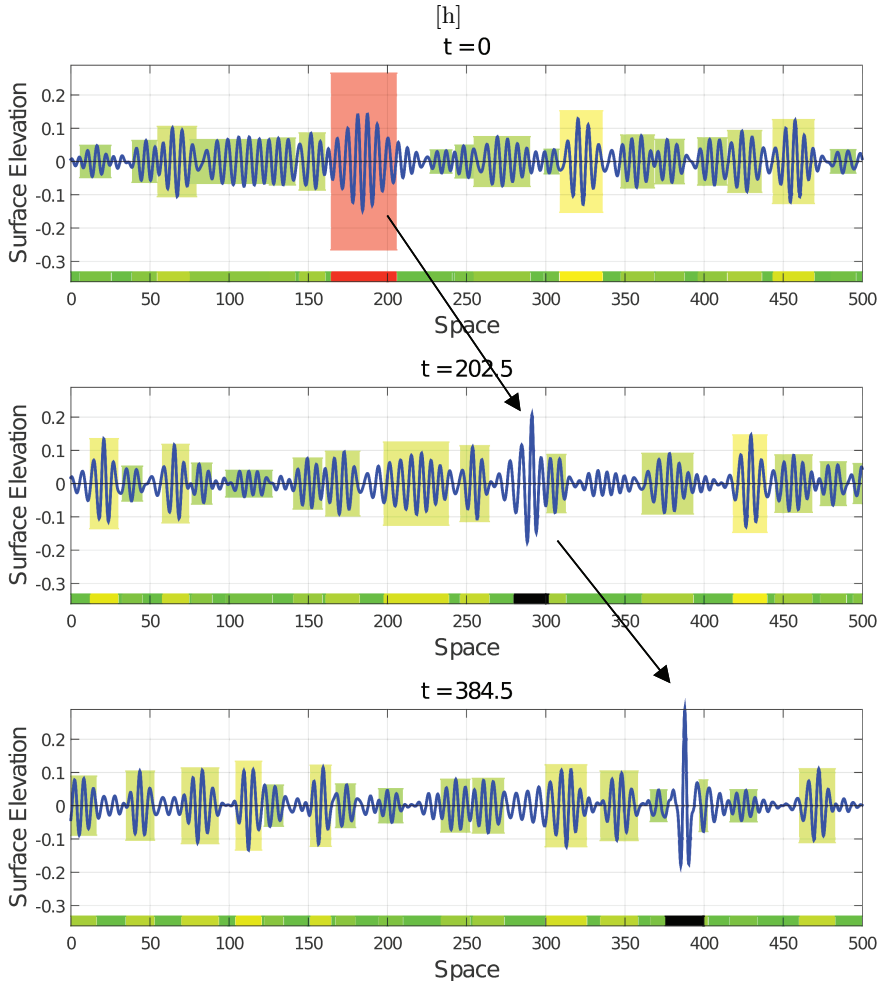
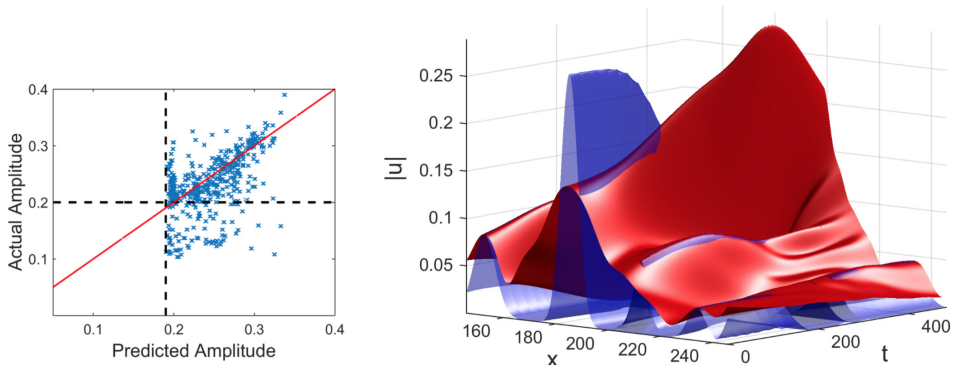


FIGURE 4. Top: Initial conditions for a simulation of MNLS. Our scheme identifies a group around $x = 190$ which we predict will grow to form a large extreme event. Middle: Group in initial stages of focusing, breaks the extreme event threshold $H_E = 0.2$ near $x = 290$. Bottom: group is fully focused and attains its maximum amplitude near $x = 390$.

($\epsilon = 0.05, \sigma = 0.1, \text{BFI} = 1.4, H_E = 0.2$). We display the spatial dependence of the surface elevation for three different values of time. In this simulation, the surface elevation first exceeds H_E around $t = 200$ near $x = 300$. After exceeding this threshold, the extreme event continues to focus, eventually reaching a maximum of approximately 0.3 at $t \approx 385, x \approx 390$ (Figure 4, bottom pane).

We highlight each wave group with a rectangle whose height is equal to the predicted focused amplitude of the group, with a red colored rectangle indicating that we predict that the group will focus to form an extreme event. Our scheme identifies the group that will ‘trigger’ the extreme event far in advance. The initial prediction occurs at the beginning of the simulation at $t = 0, 200$ time units (≈ 32 temporal wave periods) before the elevation crosses the extreme event threshold $H_E = 0.2$, and nearly 400 time units before the extreme event reaches its maximal amplitude. Perhaps most importantly, the prediction occurs while the elevation is at the relatively modest value of 0.147.

Also, our scheme accurately gives the spatiotemporal location where the extreme event



[h]

FIGURE 5. Left: scatterplot of predicted/actual amplitudes as well as the line predicted=actual (red). Note that the vertical dashed line is located at $0.95H_E$ to reduce false negatives (as discussed in the text). Right: spatiotemporal dependence of $|u|$ (red) and predicted future amplitude (blue).

will occur. The group that we predict will focus to an extreme event (red rectangle in Figure 4, top pane), has a length scale of 10.3 and amplitude 0.147. In MNLS, a localized hyperbolic secant initial profile with these characteristics will focus to a maximum amplitude of 0.264 after 351 time units, meaning that our scheme predicts a wave of this amplitude at $t = 351, x = 361$. To predict this spatial location we use the linear group velocity and the fact that the group is located at $x = 185$ initially. This agrees well with the observed dynamics of the simulation of the full field using MNLS—the identified group focuses to an actual maximum of 0.289.

To test the reliability of this scheme, we implemented it on 100 simulations each of NLS and MNLS with $BFI = 1.4$ (see Appendix A for details on these simulations). Here we only discuss the MNLS results, as the NLS results are similar and MNLS is the more physically relevant equation. In these 100 simulations, there were 336 extreme events. We predicted all of these extreme events in advance—there were no false negatives. There were 91 instances where we predicted an extreme event but one did not occur, giving a false positive rate of 21.3%. For our correct predictions, the average warning time (the amount of time before the prediction began and the onset of the extreme event) was 153 time units (≈ 24 temporal wave periods).

Our scheme has value beyond a binary predictor of extreme events. In the left pane of Figure 5, we display a scatter plot showing the relationship between the predicted future amplitude and the actual future amplitude of the wave field. We observe that our predictor reliably estimates the future amplitude in a continuous sense. In addition to predicting when an upcoming extreme event is likely, our scheme predicts when a particularly *large* extreme event is upcoming.

To further illustrate the skill of our scheme, in the right pane of Figure 5, we plot the surface $|u(x, t)|$ in red, as well as the predicted future group shape in blue. The field displayed here is the same field displayed in Figure 4 in a coordinate frame moving with the linear group velocity. The surface plots in Figure 5 provide a visualization of the skill of our scheme in predicting the future amplitude of the extreme wave, as well as the spatial location at which it will occur. The blue surface near the extreme event decays and vanishes around $t = 200$ is because we locally turn off the predictor while an extreme event is occurring ($|u| > H_E$).

5.2. Prediction by Gabor Projection

We now describe an alternative reliable prediction scheme that requires negligible computational cost. In this scheme, we predict upcoming extreme events by projecting the field onto a set of carefully tuned Gabor modes. This approach is similar in spirit to our extreme event predictive scheme for the model of Majda, McLaughlin, and Tabak (MMT) (Cousins & Sapsis 2014). This projection requires only a single convolution integral, so its computation is extremely cheap. Even at this low cost, this scheme reliably predicts upcoming extreme events with spatiotemporal skill.

As we showed in Section 3, for a given spectrum we can compute the joint density of wave group amplitude and length scale. Using our study of isolated localized groups, we can then compute the conditional density of wave group properties for groups that will ‘trigger’ extreme events. This gives the density of group length scales for groups that would focus to form an extreme event (refer to Figure 3, right column). From this, we can compute the spatial length scale L_G with the maximum likelihood of ‘triggering’ an extreme event. Due to the narrowness of the distribution of extreme event-triggering group length scales, we expect that extreme events will be preceded by energy localization at a length scale close to L_G .

To predict extreme events, we estimate the energy concentrated in scale L_G . To do so, we “project” the field onto the set of Gabor basis functions $v_n(x; x_c)$, complex exponentials multiplied by a Gaussian window function. This gives the the Gabor coefficients $Y_n(x_c, t)$:

$$v_n(x; x_c) = e^{i\pi n(x-x_C)/L_G} \exp\left[-\frac{(x-x_C)^2}{2L_G^2}\right],$$

$$Y_n(x_c, t) = \langle u(x, t), v_n(x; x_c) \rangle / \langle v_n(x; x_c), v_n(x; x_c) \rangle.$$

We claim that a large value of Y_0 at a spatial point x_c indicates that an extreme event is likely in the future near x_c in space (in a frame moving with the group velocity). To confirm this, we compute the following family of conditional distributions.

$$F_{Y_0}(\mathcal{U}) \triangleq \mathcal{P}\left(\begin{array}{c} \max_{\substack{|x^*-x_c| < L_G \\ t^* \in [t+t_A, t+t_B]}} |u(x^*, t^*)| > \mathcal{U} \mid |Y_0(x_c, t)| = \mathcal{Y}_0 \end{array}\right). \quad (5.1)$$

That is, given a particular current value of Y_0 , we examine what are the statistics of the envelope u in the future. Here we choose $t_A = 50$ and $t_B = 350$ from the time required for a group of length scale of L_G to focus to form an extreme event. We compute the statistics (5.1) from 200 simulations of NLS/MNLS with Gaussian spectra and random phases with $\epsilon = 0.05$, $\sigma = 0.1$, $\text{BFI} = 1.4$.

In the left pane of Figure 6, we display the family of conditional densities of future $|u|$ for a range of values of $|Y_0|$. These densities show that when $|Y_0|$ is large, $|u|$ is essentially guaranteed to be large in the future. From these conditional statistics, we compute the probability of an upcoming extreme event P_{EE} as a function of current Y_0 by integrating over (H_E, ∞) . This function is displayed in the right panel of Figure 6. P_{EE} has a sigmoidal dependence on Y_0 : if Y_0 is large enough than an upcoming extreme event is nearly guaranteed, while if Y_0 is small enough than an upcoming extreme event is highly unlikely.

Our predictor Y_0 becomes large distinctly *before* the extreme event occurs. The con-

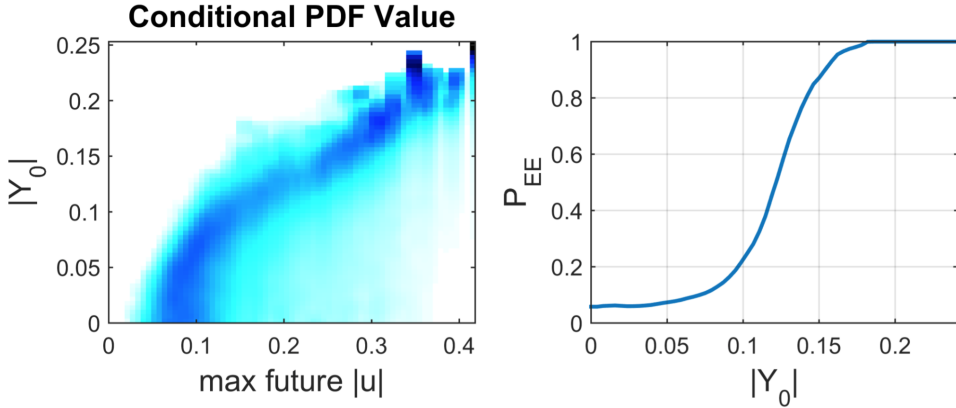


FIGURE 6. Left: Family of conditional densities of current $|Y_0|$ and future $|u|$, corresponding to (5.1). Right: probability of upcoming extreme event as a function of $|Y_0|$

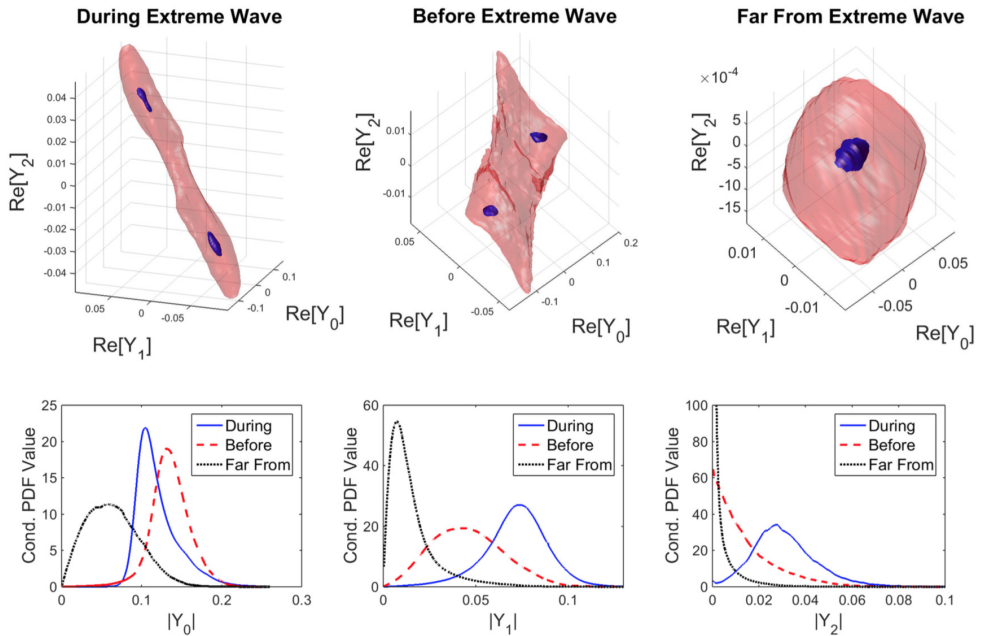


FIGURE 7. Top: Level surfaces of the joint density of the real parts of Y_0, Y_1 , and Y_2 during (left), before (middle) and far from (right) an extreme event. Bottom: marginal statistics of Y_0 (left), Y_1 (middle), and Y_2 (right) during, before, and far from an extreme event.

ditional statistics shown in Figure 6 pair a value of Y_0 with a maximum value of $|u|$ which occurs at least $t_A = 50$ time units in the future. To further illustrate this point, we statistically investigate the energy exchanges between the various Gabor modes. To do so, we compute the statistics of the Gabor coefficients during, before, and far from an extreme event. We display these Gabor statistics in Figure 7. We see that away from extreme events, we have nearly Gaussian statistics for the coefficients. In this regime the coefficients also appear to be uncorrelated. Before an extreme event, the coefficients are larger— Y_0 in particular is quite large. During an extreme event, Y_0 is on average *smaller* than before extremes (see Figure 7, bottom left). In the formation of the extreme events,

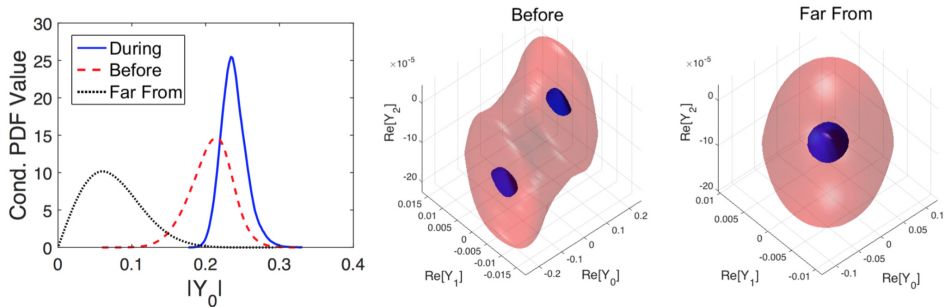


FIGURE 8. Marginal statistics of Y_0 computed for $1D$ linear waves (MNLS equation without nonlinear terms) during, before, and far from an extreme event. The corresponding level surfaces of the joint density of the real parts Y_0, Y_1 , and Y_2 are also shown.

Y_0 decreases by transferring energy to Y_1 , which is largest during the extreme events. During the extreme events, the Gabor coefficients are also strongly correlated (Figure 7, top left) presenting essentially non-Gaussian behavior.

For reference we compare the marginal statistics of Y_0 computed previously with MNLS with the corresponding linear equation, i.e. MNLS with the same parameters but without nonlinear terms (Figure 8). We find that in the linear case rare events are also preceded by large Gabor coefficients Y_0 , which follow an essentially non-Gaussian distribution. However, in this case Y_0 is much larger compared with the nonlinear case since the amount of amplification is much smaller (due to the absence of modulation instability). This implies that in both the linear and nonlinear wave models, extreme events are preceded by localized wave groups. This is an important property that can lead to rare event prediction for weakly nonlinear wave fields where modulation instability is not relevant.

To predict extreme events, we first compute Y_0 by convolving the field u with a Gaussian with the length scale L_G tuned to the particular spectrum. After computing Y_0 , we then compute the probability of an upcoming extreme event via our pre-computed conditional statistics (Figure 6, right). We predict that an extreme event will occur if $P_{EE} > P^*$, where P^* is a threshold probability that we choose. Choosing a large P^* will result in few false positives and many false negatives, while choosing a small P^* will result in few false negatives and many false positives. We choose $P^* = 0.5$ as it gives a low rate of false negatives (meaning we predict almost all extreme events) with a reasonably low false positive rate.

In Figure 9, we display the output of the Gabor predictive scheme applied to an example extreme event in a simulation of MNLS (this is the same example we investigated for the group detection-based predictive scheme in Figure 4. The extreme event that occurs at $x \approx 390, t \approx 385$ is predicted from the initial conditions by our Gabor-based predictive scheme, with a high level of confidence ($P_{EE} = 0.965$). This prediction occurs 200 time units (32 wave periods) before the amplitude exceeds H_E , and 385 time units (61 wave periods) before the maximally focused amplitude. The spatial location of the upcoming extreme event (in a moving coordinate frame) is predicted with very good accuracy as well.

To assess the reliability of this scheme, we tested it on the 100 MNLS simulations used to test the group detection-based scheme in the previous section. None of these simulations were used to generate the conditional statistics in Figure 6. We give data describing the performance of both predictive schemes in Table 1. The Gabor scheme

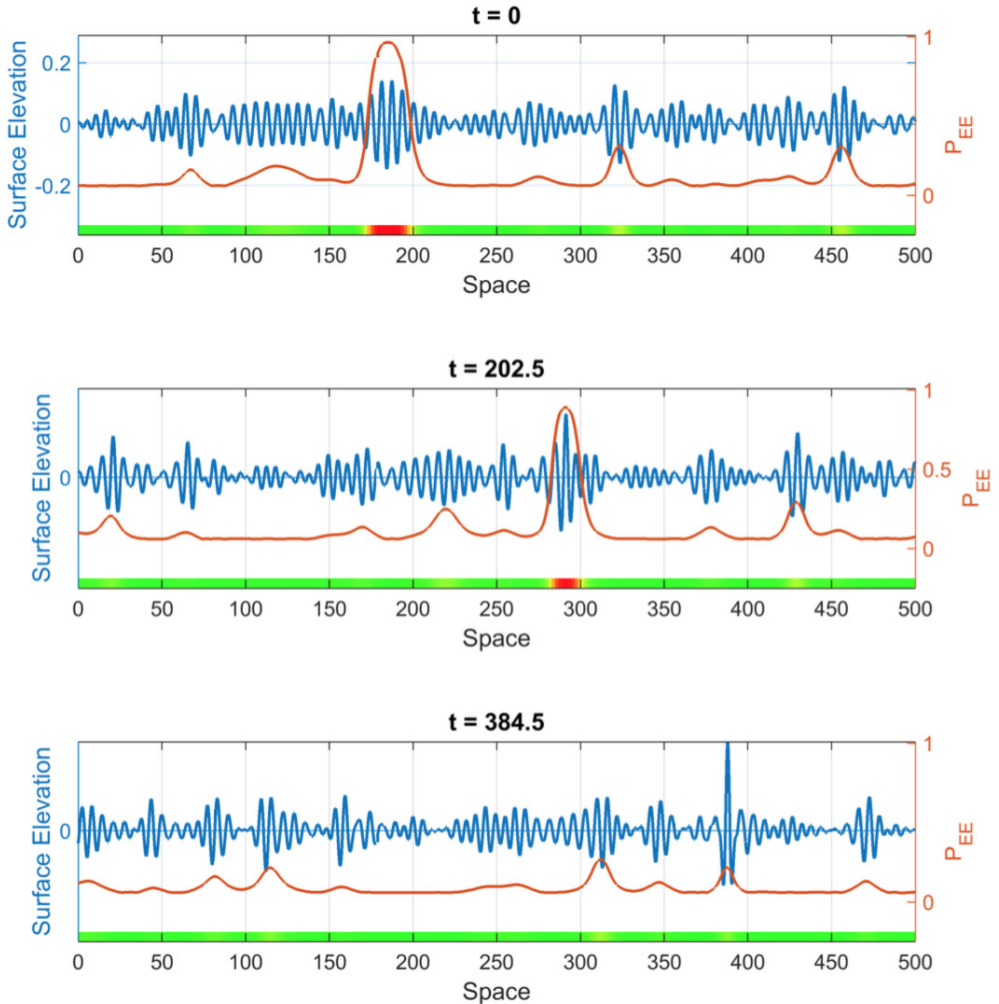


FIGURE 9. Surface elevation (blue) and probability of upcoming extreme event (red) for $t = 0$ (top), $t = 202.5$ (middle), and time at which maximum elevation attained, $t = 384.5$ (bottom).

predicted 316 of the 336 extreme events giving a low false negative rate of 5.9%. There were 108 instances where the Gabor scheme predicted an extreme event but one did not occur, giving a false positive rate of 25.5%. Thus, the Gabor scheme has a slightly higher false positive/negative rate compared with the group detection scheme but overall it performs nearly as well while requiring extremely little computational effort. Additionally, the average warning time for the Gabor scheme was larger than the group detection scheme (245 vs 153 time units, 39 vs 24 temporal wave periods).

We tested both prediction algorithms using a Gaussian spectrum with wider characteristics ($\epsilon = 0.05, \sigma = 0.2$), as well as, a JONSWAP spectrum given by:

$$S(k) = \frac{\alpha}{2k^3} e^{-(3/2)[k_0/k]^2} \gamma \exp[-(\sqrt{k} - \sqrt{k_0})^2 / 2\delta^2 k_0]$$

where $\delta = 0.07$ for $k \leq k_0$, $\delta = 0.09$ for $k > k_0$. For the JONSWAP spectrum we set

Predictive Scheme	Extreme Events	False Neg.	False Pos.	Avg. Warning Time
Gaussian Spectrum ($\epsilon = 0.05, \sigma = 0.1$)				
Gabor	336	20 (5.9%)	108 (25.5%)	245 (39 periods)
Group Detection	336	0	91 (21.3%)	153 (24 periods)
Gaussian Spectrum ($\epsilon = 0.05, \sigma = 0.2$)				
Gabor	342	29 (8.5%)	121 (26.1%)	193 (31 periods)
Group Detection	342	7 (2.0%)	111 (24.5%)	74 (12 periods)
JONSWAP Spectrum				
Gabor	383	7 (1.8%)	139 (27.0%)	237 (38 periods)
Group Detection	383	14 (3.7%)	115 (23.1%)	70 (11 periods)

TABLE 1. Performance of Gabor and group detection prediction schemes on 100 simulations of MNLS.

$\gamma = 6$ and choose α so that the significant wave height is 0.2. The results are presented in Table 1 and indicate the robustness properties of both predictive schemes.

6. Discussion

We have studied and quantify how energy localization (induced by the linear dispersive mixing of waves) and strong local nonlinearity (having the form of modulation instability of localized wave groups) interact, resulting in the ‘triggering’ of extreme waves. Based on this analysis we have developed two methods to derive precursors of rare events in nonlinear waves. The first method relies on the prediction by a wave group identification method. Specifically, we combined i) nonlinear modulation instability results that quantify the focusing of localized wave groups and ii) a scale-selection algorithm that detects wave groups that satisfy this localized stability criterion. This scheme allows us to detect efficiently and without solving the governing equations wave groups having high probability of ‘triggering’ an extreme wave. Most importantly, the developed precursor can foresee an extreme event *before* the amplitude of the wave field becomes important.

The second method relies on the tracking of energy localized over a critical length scale. We used the scale-selection algorithm to quantify, for a given wave spectrum, the probability of the formation of critical wave groups that can evolve into rare events. This analysis revealed a spatial length scale, where important energy has the highest likelihood to ‘trigger’ a rare event. Based on this result, we formulated an even simpler predictor relying on the Gabor transform, which locally tracks the energy of the wave field over the critical length scale. We applied the two predictive schemes in the MNLS equation to forecast rare events in directional water waves. Both precursors reliably predicted rogues in advance. Most importantly, this prediction was robust against noise in the background field, allowing for reliable forecast of, on average, 12-39 wave periods before the occurrence of an extreme wave, depending on the initial spectrum.

Note that although we considered (for demonstration purposes) unidirectional deep water waves, where heavy tails are more prominent, there are no constraints for the

presented theory to be applied in other setups involving the occurrence of rare events due to dynamical instabilities. Indeed, heavy-tailed statistics is not a strict requirement for our scheme. The presented approach introduces a new paradigm for understanding and inexpensively predicting intermittent and localized events in general dynamical systems where we have an interplay between uncertainty and nonlinearity. For such systems previous analytical studies have mainly focused on the quantification aspects of rare event statistics through the use of generalized Pareto distribution (see e.g. Lucarini *et al.* (2012), Lucarini *et al.* (2014)). As our approach uses minimal analytical tools, we believe it may be utilized for both prediction and statistical quantification in settings where the dynamics are exceedingly complicated or entirely unknown (requiring a data driven approach).

In the future, we plan to examine precursors of rare events for two-dimensional water waves, waves in regions with variable bathymetry, as well as waves in crossing seas. Deriving inexpensive precursors of strongly nonlinear instabilities will allow for the improvement of direct numerical methods (see e.g. Clauss *et al.* (2014), Alam (2014)) for short term prediction of the wave field evolution through the use of adaptive resolution techniques. To this end, we plan to combine the presented precursors with existing prediction schemes formulated for linear and weakly non-linear equations in order to improve their efficiency by placing more computational effort in spatiotemporal regimes where strongly nonlinear interactions are expected.

Acknowledgments: This research has been partially supported by the Naval Engineering Education Center (NEEC) grant 3002883706 and by the Office of Naval Research (ONR) grant ONR N00014-14-1-0520. The authors thank Amin Chabchoub, Francesco Fedele, Pierre Gremaud, and Craig Merrill (NEEC Technical Point of Contact) for stimulating discussions. They also thank the anonymous referees for numerous comments and suggestions that led to important improvements.

Appendix A. Scale Selection Algorithm

Here we describe the wave group detection algorithm used in the prediction scheme discussed in Section 55.1. To find the dominant wave groups in a given irregular wave field, we look for Gaussian-like “blobs” in $|u(x)|$. To find these blobs, we use an existing algorithm based on the scale normalized derivatives of $|u|$ (Koenderink 1984; Witkin 1984; Lindeberg 1998). These scale-normalized derivatives, $s^{(m)}$, are normalized spatial derivatives of the convolution of $|u|$ with the heat kernel:

$$s^{(m)}(x, L) = L^{m/2} \frac{\partial^m}{\partial x^m} (f * g)$$

where $g(x, L)$ is the heat kernel:

$$g(x, L) = \frac{1}{\sqrt{2\pi L}} e^{-\frac{x^2}{2L}}.$$

in the above, x is the spatial variable and L is the length scale variable. Following (Lindeberg 1998) we choose $m = 2$ for optimal blob detection.

We illustrate this approach by computing the scale-normalized derivatives of a single Gaussian: $u(x) = Ae^{-x^2/2L_0^2}$. It is straightforward to show that $s^{(2)}$ has a local minimum at $x = 0, L = 2L_0^2$. In an arbitrary field $|u|$, we similarly find wave groups by computing $s^{(2)}$ and subsequently find the local minima. If we find a local minima at (x_C, L^*) , we

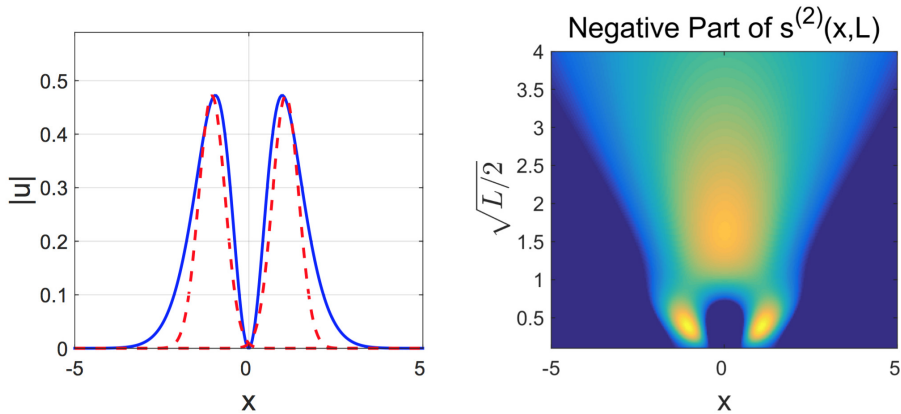


FIGURE 10. Left: Plot of double-humped field $|u|$ and the groups identified via the scale selection algorithm. Right: Negative part of $s^{(2)}$. The extremum at $x = 0, \sqrt{L}/2 = 2$ is eliminated via the procedure described in the text.

conclude that there is a wave group at $x = x_C$ having a length scale $\sqrt{L^*/2}$. We determine the amplitude of the wave group, A , by computing the local maxima of $|u|$ near x_C .

In some instances, scale space extrema do not correspond to actual wave groups. Consider $u(x) = e^{-x^2/2L_0^2} - e^{-x^2/2L_1^2}$, where $L_1 = 0.8L_0$, displayed in the left pane of Figure 10. There are two distinct peaks, which the scale selector detects. However, there is an additional local minimum of $s^{(2)}$ near $x = 0$ that does not correspond to a wave group. To eliminate such false positives, for each local minimum of s_2 , we compute the quantity C , which measures how close u is to a Gaussian-like blob:

$$C = 1 - \frac{\|f(x) - Ae^{-(x-x_C)^2/2(L^*)^2}\|_2}{\|Ae^{-(x-x_C)^2/2(L^*)^2}\|_2}$$

if $|u|$ is an exact Gaussian, then C is 1. Thus, we take small values of C as evidence that the local minimum of $s^{(2)}$ do not correspond to a wave group. In the two-humped case displayed in Figure 10, the two local minima around $x = -1, 1$ have $C \approx 0.9$, while $C \approx 0.5$ at $x = 0$. In practice, we ignore local minima of $s^{(2)}$ where $C < 0.75$. An example output of the scale selection algorithm with this criteria applied to an irregular wave field is displayed in the top pane of Figure 3. We see that the algorithm successfully identifies the dominant wave group in the field.

To compute the local minima of $s^{(2)}$, we first generate initial guesses for the minima by computing $s^{(2)}$ on a grid with $N_{x,SS}$ spatial points and N_L points in the length scale dimension. We then refine the local minima of the grid-evaluated $s^{(2)}$ by Newton's method. For a particular length scale value L , computation of $s^{(2)}(\cdot, L)$ requires two fast Fourier transforms. Thus, the cost is $\mathcal{O}(N_L N_{x,SS} \log N_{x,SS})$. We have found that a relatively small N_L is adequate to generate reliable initial guesses for the minima (we use $N_L = 20$).

For the Newton iteration, we compute the gradient and Hessian of $s^{(2)}$ analytically (these analytic expressions do contain integral terms, which we evaluate numerically). For each wave group, we refine (x_C, L) to five digits of precision, which requires no more than 3 Newton iterations in almost all cases. Note that compared to the grid computation of $s^{(2)}$, the cost of the Newton iterations is low. The reason for this is that at each iteration

the gradient and Hessian of $s^{(2)}$ need only be calculated at a single point. This means that the associated integration is only over a small subset of the full spatial domain.

Prediction via this scale selection algorithm is considerably cheaper than solving the envelope PDE. In the example considered in Figure 55.1, we predict an extreme event 200 time units in advance using the scale selection-based algorithm. Evolving the field this many time units with the PDE would require thousands of time steps, each costing $\mathcal{O}(N_{x,PDE} \log N_{x,PDE})$ to compute the nonlinear terms, where $N_{x,PDE}$ is the number of spatial grid points in the numerical PDE solver. By contrast, the scale selection algorithm only requires $N_L = 20$ evaluations of $s^{(2)}(\cdot, L)$, with each evaluation of $s^{(2)}(\cdot, L)$ requiring $\mathcal{O}(N_{x,SS} \log N_{x,SS})$ operations. To accurately resolve the small scale dynamics and the nonlinear terms, $N_{x,PDE}$ must be considerably greater than $N_{x,SS}$, which demonstrates clearly the computational gain of the proposed approach (for the considered setting we found that $N_{x,SS}$ can be 16 times smaller than $N_{x,PDE}$ with no loss of reliability).

REFERENCES

- ADCOCK, T. A. A., GIBBS, R. H. & TAYLOR, P. H. 2012 The nonlinear evolution and approximate scaling of directionally spread wave groups on deep water. *Proc. R. Soc. A* **468**, 2704–2721.
- ADCOCK, T. A. A. & TAYLOR, P. H. 2009 Focusing of unidirectional wave groups on deep water: an approximate nonlinear Schrodinger equation-based model. *Proc. R. Soc. A* **465**, 3083–3102.
- AKHMEDIEV, N. & PELINOVSKY, E. 2010 Editorial – Introductory remarks on ‘Discussion and Debate: Rogue Waves – Towards a Unifying Concept?’. *Eur. Phys. J. Special Topics* **185**, 1–4.
- ALAM, M.-R. 2014 Predictability horizon of oceanic rogue waves. *Geophysical Research Letters* **41** (23), 8477–8485.
- ALBER, I. E. 1978 The effects of randomness on the stability of two-dimensional surface wavetrains. *Proceedings of the Royal Society of London. A. Mathematical and Physical Sciences* **363** (1715), 525–546.
- BENJAMIN, T. B. & FEIR, J. E. 1967 The disintegration of wave trains on deep water. *J. Fluid. Mech.* **27**, 417–430.
- BERLAND, H., SKAFLESTAD, B. & WRIGHT, W. M. 2007 EXPINT–A MATLAB package for exponential integrators. *ACM Transactions on Mathematical Software (TOMS)* **33** (1), 4.
- BOCCOTTI, P. 1983 Some new results on statistical properties of wind waves. *Applied Ocean Research* **5** (3), 134–140.
- BOCCOTTI, P. 2008 Quasideterminism theory of sea waves. *Journal of Offshore Mechanics and Arctic Engineering* **130** (4), 41102.
- CHABCHOUB, A., HOFFMANN, N., ONORATO, M. & AKHMEDIEV, N. 2012 Super rogue waves: observation of a higher-order breather in water waves. *Physical Review X* **2** (1), 11015.
- CHABCHOUB, A., HOFFMANN, N., ONORATO, M., GENTY, G., DUDLEY, J. M. & AKHMEDIEV, N. 2013 Hydrodynamic supercontinuum. *Physical review letters* **111** (5), 054104.
- CHABCHOUB, A., HOFFMANN, N. P. & AKHMEDIEV, N. 2011 Rogue wave observation in a water wave tank. *Physical Review Letters* **106** (20), 204502.
- CHOI, W. & CAMASSA, R. 1999 Exact evolution equations for surface waves. *Journal of engineering mechanics* **125** (7), 756–760.
- CLAUSS, G. F., KLEIN, M., DUDEK, M. & ONORATO, M. 2014 Application of Higher Order Spectral Method for Deterministic Wave Forecast. In *Volume 8B: Ocean Engineering*, p. V08BT06A038. ASME.
- COUSINS, W. & SAPSIS, T. P. 2014 Quantification and prediction of extreme events in a one-dimensional nonlinear dispersive wave model. *Physica D* **280**, 48–58.
- COUSINS, W. & SAPSIS, T. P. 2015 The unsteady evolution of localized unidirectional deep water wave groups. *Physical Review E* **91**, 063204.
- COX, S. M. & MATTHEWS, P. C. 2002 Exponential time differencing for stiff systems. *Journal of Computational Physics* **176** (2), 430–455.

- CRAIG, W. & SULEM, C. 1993 Numerical simulation of gravity waves. *Journal of Computational Physics* **108** (1), 73–83.
- CRAWFORD, D. R., SAFFMAN, P. G. & YUEN, H. C. 1980 Evolution of a random inhomogeneous field of nonlinear deep-water gravity waves. *Wave motion* **2** (1), 1–16.
- DOMMERMUTH, D. G. & YUE, D. K. P. 1987 A high-order spectral method for the study of nonlinear gravity waves. *Journal of Fluid Mechanics* **184**, 267–288.
- DYACHENKO, A. & ZAKHAROV, V. 2011 Compact equation for gravity waves on deep water. *JETP letters* **93** (12), 701–705.
- DYACHENKO, A. I., KUZNETSOV, E. A., SPECTOR, M. D. & ZAKHAROV, V. E. 1996 Analytical description of the free surface dynamics of an ideal fluid (canonical formalism and conformal mapping). *Physics Letters A* **221** (1), 73–79.
- DYSTHE, K., KROGSTAD, H. E. & MÜLLER, P. 2008 Oceanic Rogue Waves. *Annu. Rev. Fluid Mech.* **40** (1), 287.
- DYSTHE, K. B. 1979 Note on a modification to the nonlinear Schrodinger equation for application to deep water waves. *Proceedings of the Royal Society of London. A. Mathematical and Physical Sciences* **369** (1736), 105–114.
- DYSTHE, K. B. & TRULSEN, K. 1999 Note on breather type solutions of the NLS as models for freak-waves. *Physica Scripta* **1999** (T82), 48.
- DYSTHE, K. B., TRULSEN, K., KROGSTAD, H. E. & SOCQUET-JUGLARD, H. 2003 Evolution of a narrow-band spectrum of random surface gravity waves. *J. Fluid Mech* **478**, 1–10.
- FEDELE, F. 2008 Rogue waves in oceanic turbulence. *Physica D: Nonlinear Phenomena* **237** (14), 2127–2131.
- FEDELE, F. 2014 On certain properties of the compact Zakharov equation. *Journal of Fluid Mechanics* **748**, 692–711.
- FEDELE, F. & TAYFUN, M. A. 2009 On nonlinear wave groups and crest statistics. *Journal of Fluid Mechanics* **620**, 221–239.
- GOULLET, A. & CHOI, W. 2011 A numerical and experimental study on the nonlinear evolution of long-crested irregular waves. *Physics of Fluids (1994-present)* **23** (1), 16601.
- GROOMS, I. & MAJDA, A. J. 2014 Stochastic Superparameterization in a one-dimensional model for wave turbulence. *Commun. Math. Sci.* **12** (3), 509–525.
- HAYER, S. 2004 A possible freak wave event measured at the Draupner jacket January 1 1995. *Rogue waves 2004* pp. 1–8.
- HENDERSON, K. L., PEREGRINE, D. H. & DOLD, J. W. 1999 Unsteady water wave modulations: fully nonlinear solutions and comparison with the nonlinear Schrodinger equation. *Wave Motion* **29**, 341–361.
- ISLAS, A. L. & SCHÖBER, C. M. 2005 Predicting rogue waves in random oceanic sea states. *Phys. Fluids* **17**.
- JANSSEN, P. A. E. M. 2003 Nonlinear Four-Wave Interactions and Freak Waves. *Journal of Physical Oceanography* **33** (4), 863.
- KASSAM, A.-K. & TREFETHEN, L. N. 2005 Fourth-order time-stepping for stiff PDEs. *SIAM Journal on Scientific Computing* **26** (4), 1214–1233.
- KOENDERINK, J. J. 1984 The structure of images. *Biological cybernetics* **50** (5), 363–370.
- LINDBERG, T. 1998 Feature detection with automatic scale selection. *International journal of computer vision* **30** (2), 79–116.
- LINDGREN, G. 1970 Some properties of a normal process near a local maximum. *The Annals of Mathematical Statistics* pp. 1870–1883.
- LIU, P. C. 2007 A chronology of freak wave encounters. *Geofizika* **24** (1), 57–70.
- LO, E. & MEI, C. C. 1985 A numerical study of water wave Modulation based on a higher-order nonlinear Schrodinger equation. *J. Fluid Mech.* **150**, 395–416.
- LUCARINI, V., FARANDA, D. & WOUTERS, J. 2012 Universal Behaviour of Extreme Value Statistics for Selected Observables of Dynamical Systems. *Journal of Statistical Physics* **147** (1), 63–73.
- LUCARINI, V., FARANDA, D., WOUTERS, J. & KUNA, T. 2014 Towards a General Theory of Extremes for Observables of Chaotic Dynamical Systems. *Journal of Statistical Physics* **154** (3), 723–750.
- MÜLLER, P., GARRETT, C. & OSBORNE, A. 2005 MEETING REPORT — Rogue Waves The Fourteenth 'Aha Huliko'a Hawaiian Winter Workshop. *Oceanography* **18** (3), 66–75.

- ONORATO, M., OSBORNE, A. R. & SERIO, M. 2002*a* Extreme wave events in directional, random oceanic states. *Phys. Fluids* **14** (4), L25.
- ONORATO, M., OSBORNE, A. R., SERIO, M. & CAVALERI, L. 2005 Modulational instability and non-Gaussian statistics in experimental random water-wave trains. *Physics of Fluids* **17**.
- ONORATO, M., OSBORNE, A. R., SERIO, M., RESIO, D., PUSHKAREV, A., ZAKHAROV, V. E. & BRANDINI, C. 2002*b* Freely decaying weak turbulence for sea surface gravity waves. *Physical review letters* **89** (14), 144501.
- OSBORNE, A. R., ONORATO, M. & SERIO, M. 2000 The nonlinear dynamics of rogue waves and holes in deep-water gravity wave trains. *Physics Letters A* **275** (5), 386–393.
- TRULSEN, K. & DYSTHE, K. B. 1996 A modified nonlinear Schrödinger equation for broader bandwidth gravity waves on deep water. *Wave motion* **24** (3), 281–289.
- WITKIN, A. P. 1984 Scale-space filtering: A new approach to multi-scale description.
- WU, G. X., MA, Q. W. & EATOCK TAYLOR, R. 1998 Numerical simulation of sloshing waves in a 3D tank based on a finite element method. *Applied Ocean Research* **20** (6), 337–355.
- XIAO, W., LIU, Y., WU, G. & YUE, D. K. P. 2013 Rogue wave occurrence and dynamics by direct simulations of nonlinear wave-field evolution. *Journal of Fluid Mechanics* **720**, 357–392.
- YUEN, H. C. & FERGUSEN, W. E. 1978 Relationship between Benjamin-Feir instability and recurrence in the nonlinear Schrodinger equation. *Phys. Fluids* **21** (8).
- ZAKHAROV, V. E. 1968 Stability of periodic waves of finite amplitude on the surface of a deep fluid. *Journal of Applied Mechanics and Technical Physics* **9** (2), 190–194.